3D Obstacle Avoidance in Adversarial Environments for Unmanned Aerial Vehicles

M. Stewart Geyer* and Eric N. Johnson†
Georgia Institute of Technology, Atlanta, GA, 30332

As unmanned aerial vehicles (UAVs) are considered for a wider variety of military and commercial applications, the ability to navigate autonomously in unknown and hazardous environments is increasingly vital to the effectiveness of UAVs. Reliable and efficient obstacle detection is a fundamental prerequisite to performing autonomous navigation in an unknown environment. Traditional two-dimensional (planar) obstacle detection techniques, though computationally friendly, are often insufficient for safe navigation through complex environments in which commanded trajectories are restricted vertically by overhanging obstacles or increases in terrain elevation. To this end, a pan/tilt-mounted laser rangefinder is explored as a means of identifying and characterizing potential obstacles in three dimensions (3D). From GPS position data and inertial sensor measurements, the filtered laser rangefinder data are transformed into local inertial coordinates and compiled into a dynamic three-dimensional grid-based mapping of the specified domain. The Georgia Tech GTMax UAV helicopter and simulation environment provide a suitable test-bed for verification of the proposed obstacle detection methodology.

Nomenclature

M	Calibrated laser rangefinder measurement
$F_i = \{x_i,y_i,z_i\}$	Inertial reference frame
$F_b = \{x_b,y_b,z_b\}$	Body reference frame
$F_r = \{x_r,y_r,z_r\}$	Laser rangefinder reference frame
$\mathbf{q} = [q_1,q_2,q_3,q_4]^T$	Attitude quaternions of F_b relative to F_i
$\mathbf{R}_o = [X_o, Y_o, Z_o]^T$	Position vector of the vehicle center of mass measured from the datum
$\mathbf{r} = [x, y, z]^T$	Position of the laser rangefinder measurement relative to the vehicle center of mass
$\mathbf{R} = [X, Y, Z]^T$	Position of the laser rangefinder measurement relative to the datum
θ_r	Laser rangefinder tilt angle
Ψ_r	Laser rangefinder pan angle
i	grid-based map row index
j	grid-based map column index

I. Introduction

UNMANNED aerial vehicles (UAVs) have become increasingly useful platforms for a variety of military and civilian applications. UAVs enjoy distinct advantages over conventional full-scale aircraft in the form of reduced size and weight, lower operating costs, increased maneuverability, and the lack of pilot safety constraints associated with manned operations. Combat support, emergency search and rescue, and aerial surveillance are particular applications which benefit greatly from the use of unmanned aerial vehicles. In many such applications, UAVs must perform complicated tasks in the absence of an on-site human operator. Ideally, the environment around a specified vehicle flight path is well known. With knowledge of the environment a priori, GPS waypoints can be generated so as to circumvent known obstacles; however, for navigation in unknown environments, additional

* Graduate Research Assistant, Aerospace Engineering, Atlanta GA, Student Member AIAA, sgeyer@gatech.edu.
† Lockheed Martin Assistant Professor of Avionics Integration, Aerospace Engineering, Atlanta GA, Member AIAA, Eric.Johnson@aerospace.gatech.edu.

capabilities are required. Without a human operator in the loop to perceive and navigate around potential hazards, the vehicle is susceptible to damage or total loss.

The concept of real-time autonomous navigation with obstacle avoidance requires a sophisticated obstacle detection system to provide path planning algorithms with updated and accurate obstacle data.[1] The obstacle avoidance problem has been investigated extensively by the robotics community in a two-dimensional (2D) framework representative of the lateral nature of maneuvers in robot navigation. These studies suggest the use of passive sensing in the form of a stereo camera for obstacle detection.[2-3] As images are captured by the camera, image processing algorithms use combinations of texture, geometry, and color recognition to identify potential obstacles within the image. While sufficient for ground robot applications, many of these vision-based methods are deficient for high-speed platforms due to their significant computational requirements.

It follows that the notion of using machine vision as a stand-alone means of obstacle detection is somewhat limited by the current state-of-the-art of computing power. While a substantial amount of work has been devoted to addressing the computational deficiencies of existing vision techniques, other researchers have taken different approaches to solving the obstacle detection problem. One such approach involves the use of a laser ranging device as an alternative and/or supplement to computer vision.

Recently, the DARPA Grand Challenge has spawned a considerable amount of research in this area with particular attention paid to High Mobility Multipurpose Wheeled Vehicles (HMMWV).[4-7] HMMWVs, much like UAVs, must negotiate hazardous environments at high speeds with a high degree of autonomy. In turn, much of the theory developed for DARPA Grand Challenge vehicles is adaptable to UAV platforms.

It is important, however, to point out some of the incompatibilities between HMMWV and UAV obstacle detection measures. The majority of HMMWV sensor systems use a LADAR Range Imaging Camera as the primary obstacle detection tool. These LADAR systems are generally positioned so that the two-dimensional laser band intersects the ground plane at a specified distance in front of the vehicle. In this configuration, an obstacle is defined by a collection of surface points which are higher than some reference ground plane.[5] This characterization is unsuitable for UAV applications where the notion of a reference ground plane for obstacle definition is not relevant. In addition, the ground vehicle navigation problem is inherently two-dimensional by nature, whereas the UAV guidance problem introduces an additional degree of freedom. For the most part, HMMWV motion is constrained to a (2D) plane parallel to the local ground—the motion is forward or backward and left or right to avoid obstacles. On the other hand, UAV navigation solutions include forward or backward, left or right, and up or down motion. Therefore, 2D obstacle mapping methods associated with HMMWV navigation must be augmented for applications involving 3D navigation.

The research presented in this paper builds upon previous work in the field of unmanned vehicle obstacle avoidance. In particular, the single-beam laser is presented as low-cost alternative to more expensive fast scan LADAR systems used for obstacle detection. Results from preliminary flight tests are presented as verification of the laser rangefinder as an effective obstacle detection device. The paper describes various laser rangefinder scanning schemes as well as a grid-based mapping method conducive to three-dimensional obstacle avoidance and path planning. Finally, the relevance and continuance of this research is described in Section IX.

II. Experimentation

The effectiveness of the proposed obstacle detection scheme is determined from simulation and flight test results. Due in large part to its low-speed flight capabilities and maneuverability, the GTMax UAV helicopter is a suitable test-bed for obstacle avoidance experimentation. In order to simulate a true hazardous environment, 3D man-made obstacles are constructed and appropriately positioned at the Georgia Tech UAV test site. The GTMax is commanded to fly series of trajectories in close proximity to these obstacles while performing active detection and dynamic mapping of the hazards.

To supplement the real-world flight test results, various other obstacle schemes are created in the simulation environment. Virtual trajectories are commanded and followed by the simulated GTMax helicopter while the virtual obstacles are detected and mapped. Accurate modeling of the pan/tilt module, the laser rangefinder, and the helicopter dynamics within the simulation environment provides a reliable means of collecting a variety of data without the time and cost associated with flight tests.

Ultimately, the effectiveness of the proposed obstacle detection method is determined by whether or not obstacles are reliably detected and mapped in real-time so as to allow for continuous trajectory tracking and/or obstacle avoidance. The following text provides an overview of the test vehicle and simulation environment used in experimentation. In addition, preliminary flight test data are presented. These preliminary results, in part, serve to validate the laser rangefinder-pan/tilt combination as an effective platform for obstacle detection.

A. Vehicle and Hardware Description

The Georgia Institute of Technology GTMax helicopter, as seen in Figure 1, is the primary vehicle for experimentation. In its nominal configuration, the GTMax research UAV is a modified Yamaha R-Max RPH equipped with dual flight computers, a differential GPS receiver, an inertial measurement unit (IMU), and a 3-axis magnetometer. An adaptive neural-network feedback controller and a sixteen-state extended Kalman filter are used to accomplish guidance and control.[8] For this particular experiment, a pan/tilt apparatus is mounted to the forward frame of the GTMax (it should be noted that vibration isolators are incorporated into the mounting hub to attenuate vibrations caused by the engine and rotor rotation).

Figure 1. GTMax Research UAV.

To allow for range of motion of the sensor, the laser rangefinder device is mounted into the pan/tilt apparatus as seen in Figure 1. Mounting the rangefinder to the pan/tilt allows the helicopter to maintain constant attitude while peripheral obstacle detection occurs. The laser rangefinder itself is an Opti-Logic RS800 model. The laser rangefinder operates at 200 Hz and is rated for measurements of up to 800 feet. The rangefinder outputs measured distance readings and interfaces with the onboard flight computer through an RS-232 compatible port.

B. Simulation Environment

The simulation environment, developed by the Georgia Tech UAV Laboratory, is programmed primarily in C/C++ and is designed to run on both Windows and Linux machines. The simulation includes the aircraft model, the aircraft interface model (Yamaha Attitude Control System or YACS), and sensor models for the IMU, GPS, sonar altimeter, magnetometer, YACS, camera, and laser rangefinder. Incorporated into the sensor models are errors, mounting location and orientation, time delays, and digital interfaces. The GTMax helicopter model has six degrees of freedom as well as engine, fuel, landing gear, pan/tilt, and rotor dynamics. The aircraft interface model simulates the servo interface functionality and the RS-232 serial interface. Figure 2 illustrates the 3D graphics window which, among other functions, displays the aircraft, the local terrain, commanded trajectories, flight paths, and the aircraft systems status panel.[9] The simulation environment allows for the real-time display of all simulated onboard data, including the virtual laser rangefinder measurements. Obstacles such as the one seen in Figure 2 can be created and manually positioned in the simulation environment. The proposed obstacle detection and avoidance algorithms are then able to be tested on these virtual obstacle clusters. Assuming sufficient accuracy of the vehicle and sensor simulation models, results from both the simulation and the flight test are used to evaluate the system performance.

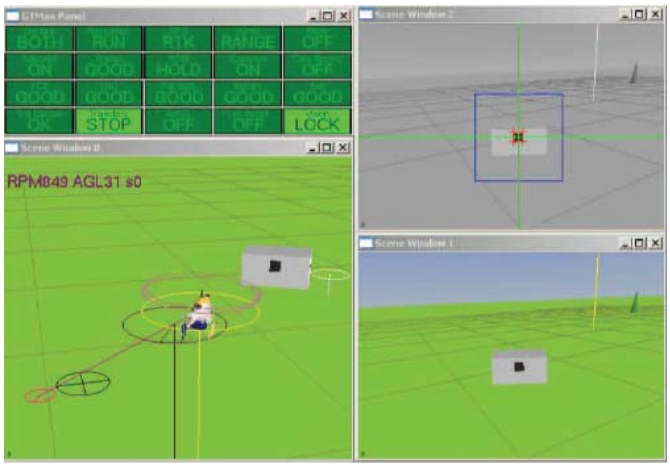

Figure 2. GTMax simulation environment.

C. Preliminary Experimental Results

A series of preliminary experiments were undertaken to evaluate the functionality of the pan/tilt and laser rangefinder systems. Specifically, the goal of these experiments was to determine the obstacle detection capabilities of the current setup and monitor the effects of helicopter vibration and auxiliary noise on laser rangefinder measurements. To accomplish these objectives, the GTMax was set in a hover at roughly 200 feet above ground level, and the pan/tilt was programmed to sweep through a series of grid coordinates overlaid onto the ground

below. Mounted to the pan/tilt apparatus of the GTMax helicopter, the laser rangefinder collected range measurements of the underlying terrain at 200 Hz. The range measurements were filtered to remove erroneous readings and converted into a local inertial coordinate frame referenced from the differential GPS tower. From laser rangefinder data, a 3D terrain mapping of the Georgia Tech UAV test site was created, as illustrated by Figure 3. The red-colored obstacles depicted in Figure 3 correspond to the test site tent and ground control truck, while the less pronounced orange peaks correspond to cars parked at the site. These on-site obstacles adequately represent the type of hazards which might be encountered in urban search and rescue missions.

The results of these tests indicate that high-resolution obstacle detection is viable for obstacles up to 200 feet away from the aerial vehicle. At this distance, the on-site hazards are readily visible and well defined as indicated by the map in Figure 3. In addition, the undulation and terrain features throughout the map are visible with relatively high resolution. The helicopter vibrations and system noise did not significantly corrupt the data—for the most part, filtering proved to be adequate for the removal of noise in the data.

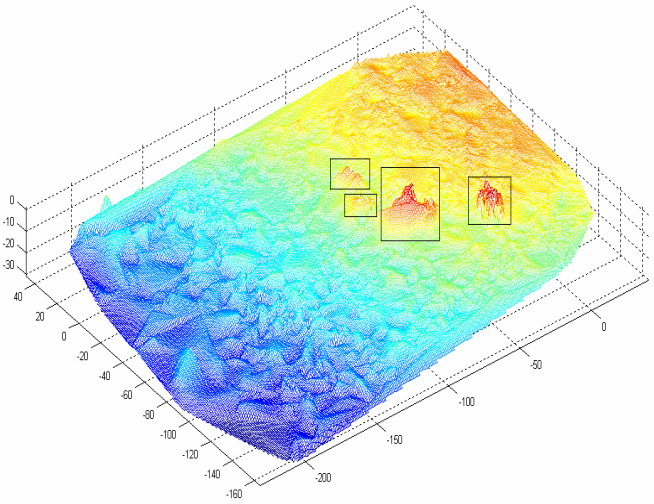

Figure 3. 3D obstacle map from laser rangefinder data.

III. Obstacle Detection

For ground vehicle applications, an obstacle is often defined as any object which extends above the ground plane by a distance which is greater than some pre-defined threshold. It follows that ground vehicles are allowed to continue through or over those objects which are smaller than the "obstacle threshold." This definition varies slightly from the more stringent definition of an obstacle required for aerial vehicle applications. For UAVs, obstacles must be defined as any objects which protrude onto the projected vehicle flight path so as to come into contact with the aerial vehicle. This is an important point to consider when adapting aspects of ground vehicle obstacle detection to aerial vehicles. Whereas contact with shrubbery and other objects might cause little or no damage to a ground vehicle, even small debris could cause substantial damage to an aerial vehicle if allowed to impact the rotor blades of a helicopter or the propeller of a fixed-wing aircraft. For this reason, thorough scanning of the surrounding environment is paramount to ensuring the safety of aerial vehicles. The following text introduces various laser rangefinder scanning schemes and describes the process of transforming range measurements into meaningful data.

A. Laser Scanning Schemes

The nominal scanning scheme exhibited in Figure 4 provides a thorough scan of the specified domain, where the bold snaking pattern represents the laser rangefinder scanning trajectory. For forward flight, the scan domain is actively re-centered about the vehicle velocity vector (indicated by the dark oval in Figure 4) to ensure that obstacles along the vehicle flight path are reliably detected. In conjunction with the grid-based mapping approach to be discussed in Section IV, collections of data are obtained from each grid cell. The thoroughness of this particular scanning scheme, however, does not come without trade-off. One disadvantage of this scheme lies in the amount of time it takes to traverse the entire domain grid-wise. This limitation could dramatically affect overall system performance since the maximum allowable autonomous flight speed is limited by the speed of obstacle detection operations. Additionally, though the grid cells immediately surrounding the velocity vector are often of primary

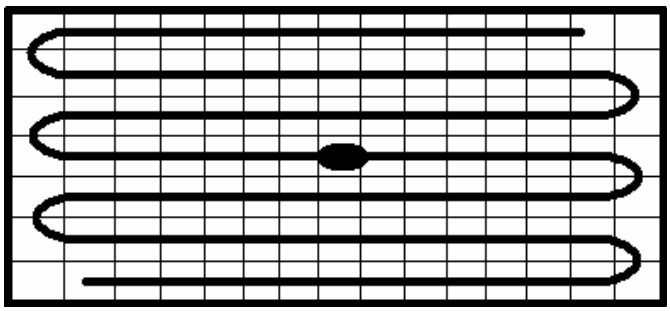

Figure 4. Nominal laser scanning scheme.

interest (since obstacles showing up in these grid cells represent imminent collision hazards), the nominal laser scanning scheme produces evenly distributed data points rather than focusing in on these specific areas.

Depending on the flight environment, alternative scanning schemes could prove beneficial. Figure 5 provides examples of various circular and elliptical scanning trajectories designed to speed up the obstacle detection process and focus more on obstacles which lie along, or in close proximity to the vehicle flight path (indicated by the shaded oval). The trajectories displayed in Figure 5 can be used individually or in parallel to provide appropriate scan coverage for the flight environment. One such hybrid scheme might consist of several cycles along the inner-most elliptical trajectory combined with intermittent switching to the outer-most trajectory to check for larger obstacles which may have entered into the domain periphery. In particular, these scanning schemes cover a significant amount of the domain in a short period of time without generating copious amounts of data per cycle. Instead of sequencing through the entire grid with data points collected from each cell, more readings can be taken in areas of interest. Though not as thorough as the nominal scanning scheme, the trajectories diagrammed in Figure 5 allow for smoother operation of the obstacle detection system.

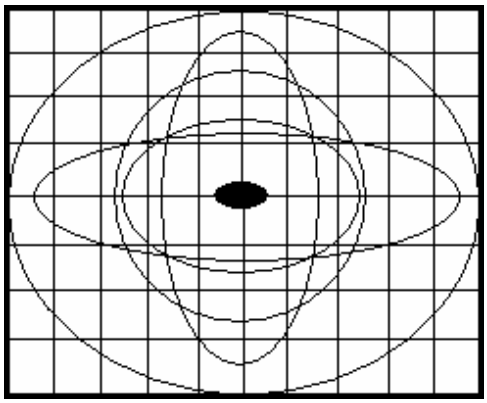

Figure 5. Various scanning schemes.

B. Coordinate Transformation

In order to construct a meaningful obstacle map, laser rangefinder measurements are expressed in a common inertial frame. For convenience, the on-site differential GPS tower is chosen as the origin of the local inertial frame. Similarly, the vehicle center of mass is chosen as the origin of the aircraft body frame. The laser rangefinder frame, denoted by subscript *r*, is referenced from the pan/tilt center with the x_r axis along the laser's optical axis. Through a series of successive coordinate transformations, laser rangefinder measurements are converted into the local inertial reference frame:

$$\mathbf{R}_r = \begin{bmatrix} M & 0 & 0 \end{bmatrix}^T \tag{1}$$

$$\mathbf{L}_{br} = \begin{bmatrix} \cos\psi_r & \sin\psi_r & 0 \\ -\sin\psi_r & \cos\psi_r & 0 \\ 0 & 0 & 1 \end{bmatrix}^T \begin{bmatrix} \cos\theta_r & 0 & -\sin\theta_r \\ 0 & 1 & 0 \\ \sin\theta_r & 0 & \cos\theta_r \end{bmatrix}^T \tag{2}$$

$$\mathbf{L}_{ib} = \begin{bmatrix} q_1^2 + q_2^2 - q_3^2 - q_4^2 & 2(q_2q_3 + q_1q_4) & 2(q_2q_4 - q_1q_3) \\ 2(q_2q_3 - q_1q_4) & q_1^2 - q_2^2 + q_3^2 - q_4^2 & 2(q_3q_4 + q_1q_2) \\ 2(q_2q_4 + q_1q_3) & 2(q_3q_4 - q_1q_2) & q_1^2 - q_2^2 - q_3^2 + q_4^2 \end{bmatrix}^T \tag{3}$$

$$\mathbf{L}_{ir} = \mathbf{L}_{ib} \cdot \mathbf{L}_{br} \qquad \mathbf{R}_i = \mathbf{L}_{ir} \cdot \mathbf{R}_r \tag{4}$$

Equation (1) represents the raw laser rangefinder measurements expressed in the *r* frame. $\mathbf{L}_{br}$ maps from the laser rangefinder frame to the vehicle body frame in the form of rotation sequences through the pan (Ψ_r) and tilt (θ_r) angles. The rotation sequence, $\mathbf{L}_{ib}$, converts vector components from the body frame to the local inertial frame. Finally, laser rangefinder measurements are transformed into the local inertial frame through the rotation matrix $\mathbf{L}_{ir}$ as illustrated in Equation (4). In this formulation, the offset between the origin of the rangefinder frame and the vehicle center of mass is assumed to be negligible. This assumption serves to reduce the number of matrix multiplications required for coordinate transformations.

IV. Obstacle Mapping

In order to extract real-time trends from the obstacle data, laser rangefinder measurements are systematically characterized and updated in a dynamic database. An adaptation of Kelly's grid obstacle map system for ground vehicles is used for representing and cataloging potential obstacles.[7] The "World Model Representation" forms the backbone of the grid-based map system; however, in the ground vehicle model, the world is projected onto a ground plane which does not allow for obstacle representation in three dimensions.[10] In order to facilitate 3D obstacle representation for UAV applications, the notion of the ground plane grid-based map is shifted from the ground plane to a plane projected in front of the aerial vehicle and normal to the velocity vector (or the heading vector in the case of stationary flight). The subsequent text describes the grid-based mapping scheme in detail.

A. Grid-Based Map

A modified version of Kelly's grid obstacle map provides a systematic means of storing laser rangefinder data. As range measurements are returned from the laser rangefinder, they are stored in a matrix data structure which mirrors the physical grid-based map projection plane. Each element of the matrix contains the range measurement location in Cartesian coordinates, its measured distance from the vehicle, and an associated confidence rating. Within the map projection plane, a window through which the vehicle can safely pass is defined. The cells encompassed by this window, and the cells immediately surrounding the window, are of particular interest. Any obstacle within this threshold represents an imminent collision hazard.

With this in mind, two criteria are employed in determining whether a grid cell (or pixel) contains an obstacle. The primary obstacle criterion consists of a check of whether an obstacle cell in the projected vehicle window is within a pre-defined distance from the vehicle. Such a scenario indicates that an obstacle lies in the vehicle flight path and is within close range of the vehicle. In this case, the associated cells receive "votes" as containing obstacles. A second obstacle detection criterion involves comparing neighboring pixel data. Standard gradient search algorithms provide a means of identifying neighboring grid cells which contain obstacles. If the difference between rangefinder measurements in adjacent grid cells, i.e. $(i - 1, j - 1)$, exceeds a pre-defined value, this cell receives a vote as containing an obstacle. The obstacle map data is continually updated in a similar manner as the laser rangefinder sweeps out the surrounding terrain.

B. Map Scrolling

As cited previously, for forward flight, the scan domain is actively re-centered about the vehicle velocity vector to ensure that obstacles along the vehicle flight path are reliably detected. This method is advantageous in that it minimizes grid relocation—the matrix data structure is expanded to include new sensor data while previous pixel data remains stored in its original map cell. In the event that the matrix data structure becomes too large (i.e. the vehicle changes heading completely) a new data structure is initialized and an obstacle map is built for the new domain.

C. Confidence Algorithm

The dynamic aspect of the grid-based map is based on the concept of confidence-based mapping.[11] In this scheme, the cell confidence increases or decreases linearly when updated by a rangefinder measurement. When a map cell receives a vote for containing an obstacle, the cell's confidence measure is increased by a pre-defined constant. When the confidence exceeds a certain threshold, the map cell is marked as an obstacle cell. If a map cell receives a conflicting vote, its confidence level decreases. This system serves to reduce the amount of false obstacle identifications as well as phase out dynamic obstacles which may have moved away from previous cell locations.

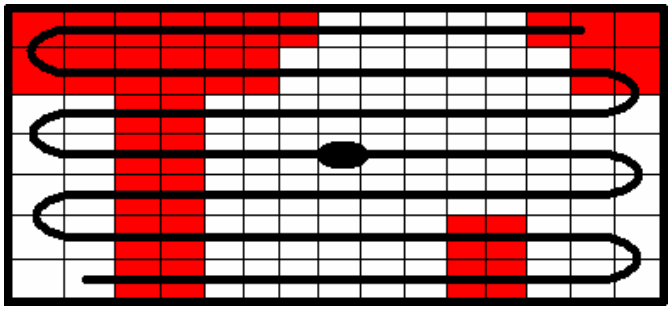

Figure 6. Obstacle map—hazard scenario.

As the obstacle detection and map builder processes are carried out, clusters of grid cells are eventually marked as "no-fly" zones. Figure 6 illustrates a possible obstacle scenario where the red cells indicate no-fly zones due to trees in the upper left- and right-hand corners, and shrubbery along the lower right portion of the scan domain. From the obstacle map, path planning algorithms are then used to steer the vehicle toward areas which are sufficiently clear of no-fly zones.

V. 2D Obstacle Avoidance

Though often insufficient for navigation in complex obstacle-rich environments, the development of two-dimensional obstacle avoidance schemes provides a logical starting point for solving the 3D avoidance problem. Whereas horizontal avoidance maneuvers are often preferable for fixed-wing vehicles, vertical avoidance maneuvers are more appropriate for VTOL (vertical take-off and landing) vehicles due to their inherent advantage in vertical thrust capability. As such, the proposed 2D avoidance scheme considers avoidance maneuvers in the vertical plane, though these strategies are equally applicable to flight in the horizontal plane. In addition, the following 2D avoidance methods are predicated upon single point laser rangefinder measurements rather than the full scale obstacle grid map detailed in Section IV.

A. Flight Modes

The proposed 2D avoidance scheme consists of three fundamental flight modes: a normal flight mode, an obstacle avoidance mode, and a return-to-path mode. The normal flight mode refers to the uninterrupted tracking of user-commanded waypoints or velocities as the laser rangefinder searches for obstacles along the vehicle's predicted path. If the obstacle avoidance mode is triggered by a detected obstacle along the predicted vehicle trajectory, the user-commanded path is pre-empted by an avoidance path generated from laser rangefinder obstacle data. Once the detected obstacle is determined to have been successfully avoided, the return-to-path flight mode initiates the reacquisition of the original user-commanded path.

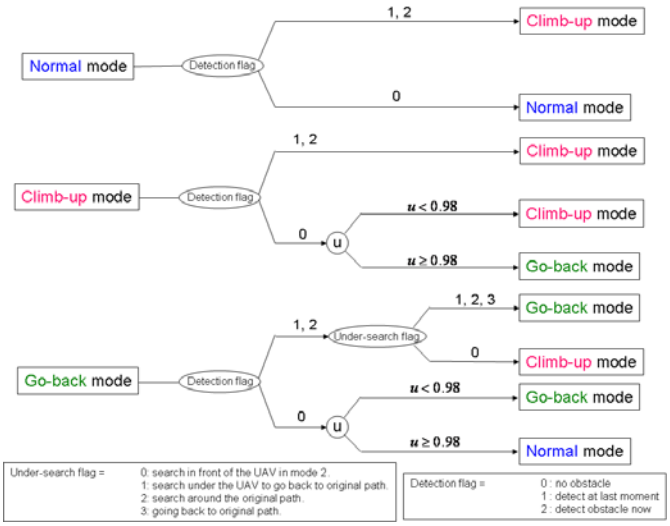

Figure 7. Avoidance mode logic tree.

Figure 7 depicts the decision tree for the various obstacle avoidance modes. The state of the "detection flag" parameter acts as the primary driver of flight mode. When a detected obstacle passes within the specified eminent collision boundary during the current or previous time step, the normal flight mode is interrupted by the avoidance mode. If no additional obstacles are detected along the predicted vehicle path after the avoidance trajectory is flown, the return-to-path mode is initiated and the original user-commanded trajectory becomes the primary flight path once again.

B. 2D Avoidance Trajectory

The 2D avoidance method is based on the strategic manipulation of the commanded vehicle path in the event of perceived obstructions along the current vehicle trajectory. For navigation in adversarial environments where performance and speed are at a premium, avoidance trajectories must be both smooth and computationally friendly. With these specifications in mind, Bézier curves provide an effective means for avoidance trajectory generation. Specifically, because Bézier curves are contained within the envelope of their control points, these points can be graphically displayed and used to manipulate the curve intuitively. Furthermore, translations, scaling, and rotations can be applied on Bézier curves, making them readily extendable to three-dimensional path planning.[12]

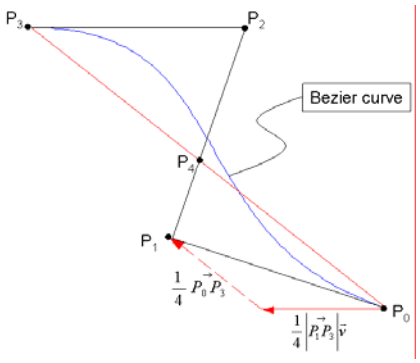

Figure 8. Cubic Bézier curve.

The general form of the parametric Bézier curve is:

$$B(u) = \sum_{i=0}^{n} P_i b_{n,i}(u), \quad u \in [0,1] \tag{5}$$

where n is the order of the Bézier curve, P_i represents the i^{th} control point, u is the parametric variable, and

$$b_{n,i}(u) = \binom{n}{i} t^i (1-t)^{n-i} \tag{6}$$

For smooth trajectory generation applications, cubic Bézier curves such as the one illustrated in Figure 8 are highly effective given their relatively low computational requirements. For n = 3, the matrix form of the Bézier curve equation is

$$B(u) = (u^3, u^2, u, 1)\begin{pmatrix} -1 & 3 & -3 & 1 \\ 3 & -6 & 3 & 0 \\ -3 & 3 & 0 & 0 \\ 1 & 0 & 0 & 0 \end{pmatrix}\begin{pmatrix} P_0 \\ P_1 \\ P_2 \\ P_3 \end{pmatrix} \tag{7}$$

The four control points—P_0, P_1, P_2, and P_3—are selected so as to generate a smooth trajectory which effectively avoids the detected obstacle. Keeping in mind that the third-order Bézier curve crosses points P_0 and P_3 but not points P_1 and P_2, it is convenient to position P_0 at the current vehicle location and it is critical to position P_3 at a point verified as safe for the vehicle to fly. Referring to Figure 8, P_4 denotes the center of P_0P_3 and is computed solely for reference purposes. Additionally, P_1 is placed at

$$P_1 = \frac{1}{4}\left|\vec{P_0P_3}\right| \cdot \left(\frac{\vec{P_0P_3}}{\left|\vec{P_0P_3}\right|} + \frac{\vec{v}}{|\vec{v}|} \right) \tag{8}$$

where v is the velocity vector of the vehicle. This selection of P_1 allows for sufficient emergent response of the vehicle. Finally, P_2 is positioned at the intersection between P_1P_4 and the horizontal line parallel to v and cross P_3. For each instance that an obstacle is detected along the generated avoidance path, the position of the "safe" point, P_3, is incremented vertically by a pre-defined value, and P_0, P_1, and P_2 are re-computed accordingly. After a sufficient number of vertical increments, P_3 is positioned safely above the detected obstacle, and the corresponding avoidance Bézier curve is flown by the vehicle.

VI. 3D Obstacle Avoidance

For navigation in and around cluttered obstacle-rich environments, the proposed 2D obstacle avoidance methods are often insufficient. Certain scenarios may, for instance, dictate the need to simultaneously navigate above and around a group of obstacles. For such scenarios, the principles of the proposed 2D avoidance methods must be expanded to encompass the three-dimensional domain.

A. Flight Modes

The primary difference between the proposed two- and three-dimensional obstacle avoidance methods is the incorporation of the grid-based obstacle map into the 3D avoidance scheme. The proposed three-dimensional avoidance scheme consists of four flight modes: a normal flight mode, a data acquisition mode, an obstacle avoidance mode, and a return-to-path mode. The definitions of the normal flight, obstacle avoidance, and return-to-path modes are the same as those of their two-dimensional counterparts; however, where the 2D avoidance strategy initiated a mandatory climb upon encountering an obstacle, the data acquisition mode of the 3D avoidance scheme seeks a definitive avoidance route by appropriately expanding the obstacle map scan domain rather than embarking upon an arbitrary avoidance trajectory. The data acquisition mode is initiated when the grid-based obstacle map consists of more than a pre-defined number obstacle cell clusters. For such a scenario, the current scan domain is deemed unsafe for passage of the vehicle, and the scan domain is successively expanded until the extended obstacle

map domain yields a feasible avoidance route. Once an appropriate avoidance route is determined, the obstacle avoidance mode is triggered, and the obstacle is successfully avoided as outlined in the following section.

B. 3D Avoidance Trajectory

As was previously stated, Bézier curves are readily extendable to three-dimensional path planning and, therefore, form the backbone of the 3D avoidance trajectory. Whereas the 2D scheme employs only single point laser rangefinder data to correctly place the Bézier control points, the 3D avoidance scheme utilizes the grid-based obstacle map discussed in Section IV to determine the "safest" location for P_3. The location of P_3 is determined from obstacle map search algorithms designed to calculate the point on the obstacle grid which minimizes susceptibility to obstacle collisions while maximizing trajectory efficiency. Once the P_3 control point location is determined from the obstacle map, the remaining control points are calculated in the same manner as the two-dimensional control points (see Equation 8 and accompanying text); however, the new Bézier curve is no longer restricted to the vertical plane. Because P_3 can be placed at any point within the obstacle grid, the avoidance Bézier curve has an additional degree of freedom allowing for more efficient obstacle avoidance. Figure 9 illustrates the difference between the proposed 2D and 3D avoidance methods. Whereas the planar restrictions on the 2D avoidance method would result in a trajectory which inefficiently goes all the way over the detected building (indicated in yellow), the 3D avoidance method yields in a more practical avoidance path as illustrated by the green curve in Figure 9.

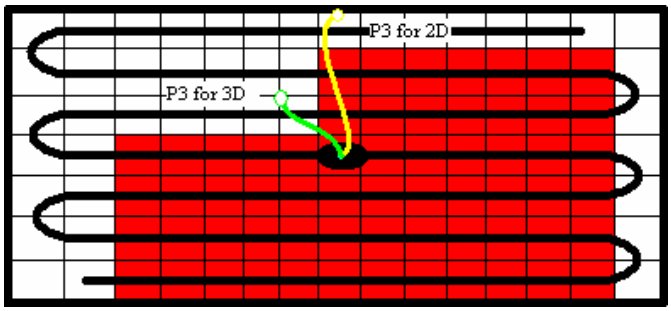

Figure 9. Difference between 3D and 2D methods.

VII. Results

Various simulation and flight tests were conducted to verify the proposed obstacle detection and avoidance methods. The subsequent text details the results of obstacle detection, 2D avoidance, and 3D avoidance experimentation.

A. Obstacle Detection

Figure 10 depicts the nominal setup used to test both the grid-wise and concentric laser rangefinder scanning schemes. For this particular setup, the virtual GTMax UAV performed stationary scans of a building at distance of roughly 100 feet. Figures 11 and 12, respectively, display results from the grid-wise and concentric laser rangefinder obstacle scan tests. The red "field-of-view" window seen in Figure 11 represents the grid-wise scan domain, while the individual blue data points depict the laser rangefinder measurements by which the building, or obstacle, is detected. Similarly in Figure 12, the blue data points show where, and to what proficiency, the concentric scanning scheme detects the building obstacle.

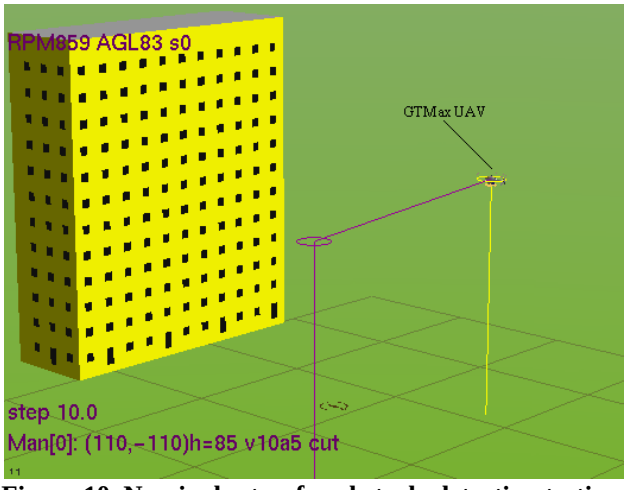

Figure 10. Nominal setup for obstacle detection testing.

Referring to Figure 11, it can be seen that the grid-wise scan scheme provides a thorough mapping of the scan domain insofar as the detected obstacle is readily identifiable with distinct boundaries. On the other hand, the proficiency of the grid-wise scan is not without consequence as the time to execute one cycle of the grid-wise scan is nearly twice the time to complete a single concentric scan cycle; however, as evidenced by Figure 12, large areas of the obstacle remain undetected as a result of the limited scope of the concentric scan scheme.

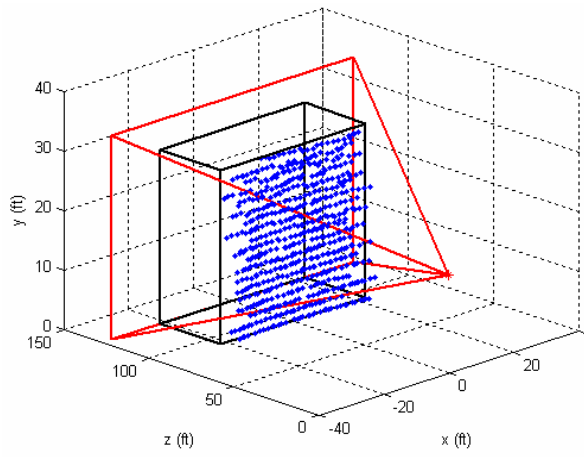

Figure 11. Grid scan of nominal building.

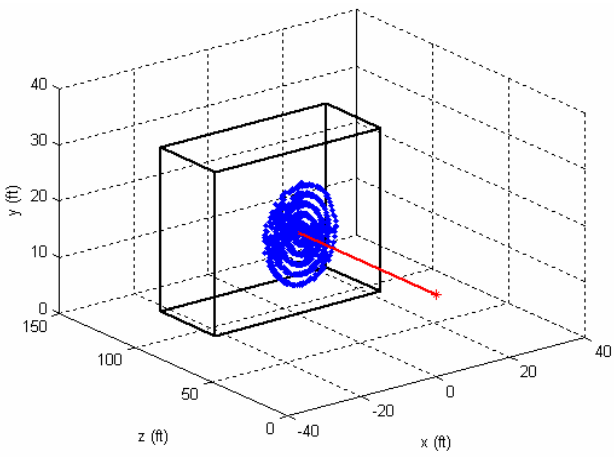

Figure 12. Concentric scan of nominal building.

B. 2D Obstacle Avoidance

The following section presents results from two-dimensional obstacle avoidance testing. The baseline mission for the 2D avoidance simulation consists of a vehicle in a constant velocity forward flight mode.

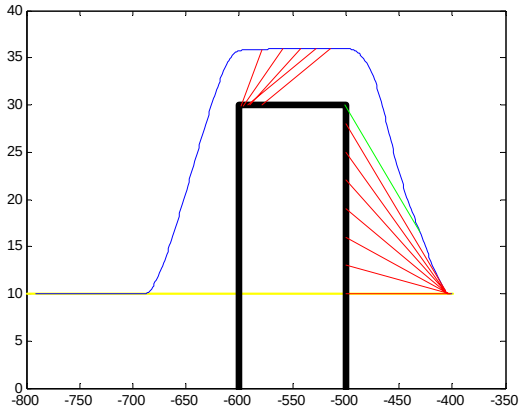

Figure 13. Single building 2D avoidance.

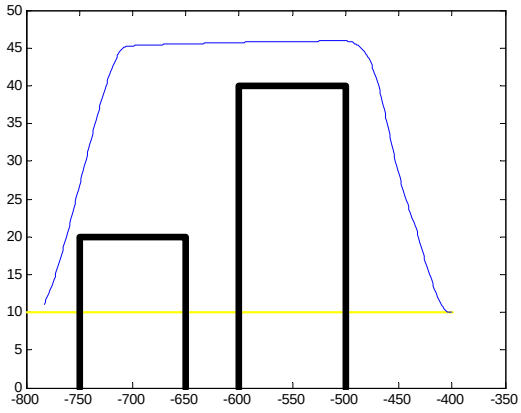

Figure 14. Multiple building 2D avoidance.

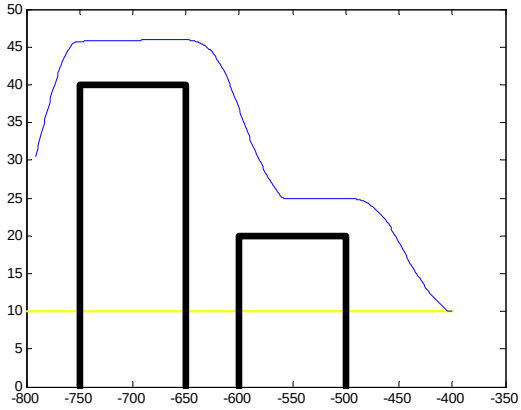

Figure 15. Avoid two sequenced buildings.

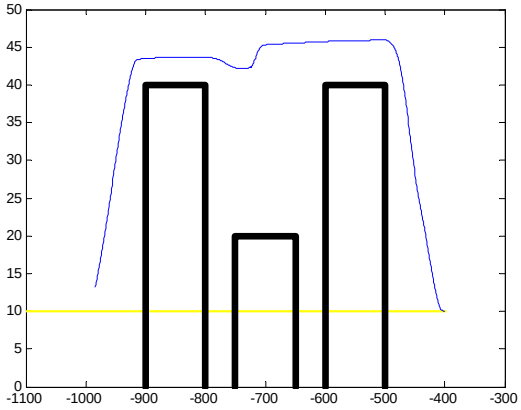

Figure 16. Avoid three sequenced buildings.

Referring to the various avoidance scenarios depicted in Figures 13-16, the blue curve represents the avoidance trajectory flown by the vehicle while the yellow path indicates the original commanded trajectory. The red-colored traces seen in Figure 13 highlight the laser rangefinder ray and the corresponding obstacle detection points. In addition, these traces serve to illustrate the successive vertical incrementing of the P_3 control point until the control point is safely above the obstacle. Furthermore, the red traces that appear on top of the building in Figure 13 depict the vehicle trying to return to the original path once the avoidance trajectory has been successfully flown. From Figures 14-16, it can be said that the proposed 2D avoidance scheme is robust to deviations from the generic single building avoidance case.

C. 3D Obstacle Avoidance

Figures 17 and 18 depict the three-dimensional obstacle scenario and avoidance path flown by the GTMax UAV in simulation. Figure 17 shows the obstacle encountered by the UAV while Figure 18 offers a view back towards the UAV from behind the detected obstacle (or building). From the grid-based obstacle map seen in the lower right-hand corner of Figure 17, the Bézier curve control point, P_3, is safely positioned in the obstacle-free notch of the

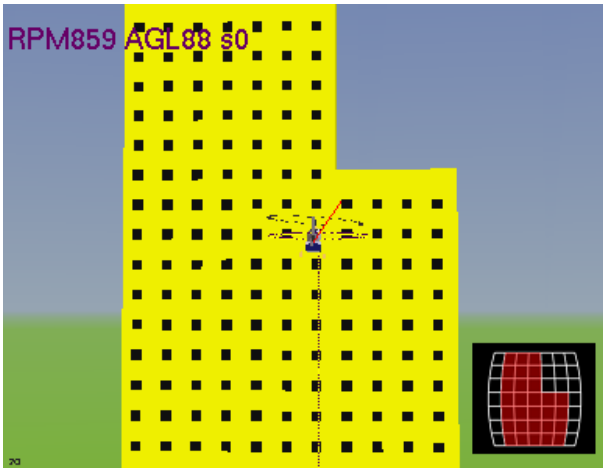

Figure 17. 3D avoidance scenario.

Figure 18. 3D avoidance trajectory.

obstructive building. From this point, the remaining Bézier control points are calculated resulting in the yellow three-dimensional avoidance trajectory seen in Figure 18. From Figure 18, it is clear that the vehicle simultaneously navigates around and over the obstructive structure rather than inefficiently attempting to climb over the highest point of the building. Furthermore, it can be seen that the generated avoidance curve is relatively smooth enabling efficient flight along the trajectory.

VIII. Conclusions

Though not as efficient as the concentric obstacle scan, the grid-based obstacle scan proved the more reliable method for faithful obstacle detection. In addition, simple pointing of the laser rangefinder along the vehicle velocity vector proved to be a surprisingly effective means of detecting obstacles during flight. Onboard vibrations and pitching motions of the vehicle served to effectively perturb the laser rangefinder beam enough to collect obstacle data from a rather broad field of view. The proposed 2D avoidance methods were proven effective in their own right; however, the ability to smartly generate avoidance trajectories with the three-dimensional avoidance approach represents a distinct advantage over the 2D avoidance schemes which are less robust and tend to break down in complex obstacle-rich environments.

IX. Future Work

A proposal for future work includes more comprehensive testing both in simulation and flight tests. In addition, methods will need to be developed to account for more complicated obstacle scenarios, such as non-convex obstacles. A final proposal for future work involves the development of a full-scale inertial obstacle map of the surrounding environment that interfaces with the local grid-based obstacle map to substantially enhance the level of autonomy of the vehicle.

Acknowledgments

The authors would like to acknowledge contributions of the following people to the work presented in this paper: Henrik Christophersen, Claus Christmann, Jason Fine, Manabu Kimura, Wayne Pickell, Nimrod Rooz, and Allen Wu. This work is supported by the Active-Vision Control Systems (AVCS) Multi-University Research Initiative (MURI) Program under contract #F49620-03-1-0401 and by the Software Enabled Control (SEC) Program under contracts #33615-98-C-1341 and #33615-99-C-1500.

References

[1]Cheng, V. H. L., and Lam, T., "Automatic Guidance and Control for Helicopter Obstacle Avoidance," *AIAA Journal of Guidance, Control, and Dynamics*, Vol. 17, No. 6, 1994, pp. 1252-1259.

[2]Zhu, Z., Lin, X., Shi, D., and Xu, G., "A Single Camera Stereo System for Obstacle Detection," *World Multiconference on Systemics, Cybernetics and Informatics - 4th International Conference on Information Systems Analysis and Synthesis*, Vol. 3, 12-16 July, 1998, pp. 230-237.

[3]Cho Y. C., and Cho H. S., "A Stereo Vision-Based Obstacle Detection Method for Mobile Robot Navigation," *Robotica*, Vol. 12, 1994, pp. 203-216.

[4]Manduchi, R., Castano, A., Talukder, A., and Matthies, L., "Obstacle Detection and Terrain Classification for Autonomous Off-Road Navigation," *Autonomous Robots*, Vol. 18, 2005, pp. 81-102.

[5]Talukder, A., Manduchi, R., Rankin, A., and Matthies, L., "Fast and Reliable Obstacle Detection and Segmentation for Cross-Country Navigation," *IEEE Intelligent Vehicles Symposium 2002*, Versailles, France, 2002.

[6]Chang, T., et. al., "Concealment and Obstacle Detection for Autonomous Driving," *Proceedings of the International Association of Science and Technology for Development – Robotics and Applications Conference*, Santa Barbara, CA, 1999.

[7]Kelly, A., "An Intelligent, Predictive Control Approach to the High-Speed Cross-Country Autonomous Navigation Problem," Ph.D. Dissertation, Robotics, Carnegie Melon University, Pittsburgh, PA, 1995.

[8]Johnson, E. N., and Schrage, D. P., "System Integration and Operation of a Research Unmanned Aerial Vehicle," *AIAA Journal of Aerospace Computing, Information, and Communication,* Vol. 1, No. 1, 2004, pp. 5-18.

[9]Wu, A. D., Johnson, E. N., and Proctor, A. A., "Vision-Aided Inertial Navigation for Flight Control," *AIAA Journal of Aerospace Computing, Information, and Communication,* Vol. 2, No. 9, 2005, pp. 348-360.

[10]Hong, T., Abrams, M., Chang, T., and Shneier, M. O., "An Intelligent World Model for Autonomous Off-Road Driving," *Computer Vision and Image Understanding*, 2000.

[11]Hong, T., Legowik, S., and Nashman, M., "Obstacle Detection and Mapping System," NISTIR 6213, August 1998.

[12]Salomon, D., "Computer Modeling & Geometric Modeling," Springer-Verlag New York, Inc., New York, NY, pp. 269-272.